JOURNAL OF MATERIALS SCIENCE 26 (1991) 6517 6521

Glass-forming ability of the Ni–B–Sn system

M. BOUDARD, B. ARCONDO, H. SIRKIN
Lab. de Sólidos Amorfos, Dpto. de Fisica, Faculdad de Ingenieria UBA, Paseo Colón 850 (1063), Buenos Aires, Argentina

The glass-forming ability (GFA) of the Ni–B–Sn ternary system has been analysed. The addition of small quantities of tin increases the GFA with relation to the Ni–B binary system. Glass formation was observed in the nickel-rich corner of the Ni–B–Sn ternary system for a tin content <15 at %. The difficulty of formation of a ternary compound $Ni_{21}B_6Sn_2$ (τ-phase) seems to play an important role in the GFA.

1. Introduction

Previous work [1, 2] shows that the addition of tin increases the glass-forming ability (GFA) of binary magnesium-based systems, which seems to be related to the strong associative tendency of tin towards magnesium. The system NiB presents two ranges of composition where the amorphous structure can be obtained by rapid quenching from the melt (a very narrow range around the eutectic at 18.4 at % in boron and the region 31–43 at % in boron) [3]. The idea was to analyse if tin added to this system played a similar role to that in magnesium-based systems and, in this case, to set the limits of glass forming composition range for the Ni–B–Sn system.

Samples belonging to the nickel-rich corner from the Ni–B–Sn system were studied. This corner presents a ternary compound with a $Cr_{21}W_2C_6$ type structure (D84), with a stoichiometric composition $Ni_{21}B_6Sn_2$ (τ phase). Fig. 1 represents the projection of the liquidus surface proposed by Stadelmaier and Jordan [4]. The primary phase field of Ni_2B was replaced by the primary field of Ni_3B. This equilibrium phase was not known at the time of Stadelmaier and Jordan's publication.

2. Experimental procedure

Alloys indicated by points A, B, C, D and E in the ternary diagram (Fig. 1), for which compositions are shown in Table I, were prepared from high-purity materials by melting under a flowing argon atmosphere using an induction furnace. Their homogeneity was checked by metallographic inspection.

Samples in ribbon form were obtained by rapid quenching by the melt-spinning technique using a 10 cm diameter copper wheel, 5500–6900 r.p.m. rotating speed, 0.3–0.38 kg cm^{-2} jet pressures, and 0.3–0.7 mm crucible orifice diameters.

Samples as-cast and as-quenched were observed by optical microscopy, X-ray diffraction (XRD), Mössbauer spectroscopy and electron probe microanalysis (EPMA). XRD was performed using copper- and cobalt-filtered radiation with a monochromator in the emergent beam in the last case. The Mössbauer studies were made using a source of SnO_3Ba at room temperature. EPMA was performed in a Cameca SX 50 equipment fitted with a wavelength-dispersive spectrometer.

The crystallization behaviour of one of the melt-spun samples (B) was studied by Mössbauer spectroscopy and XRD.

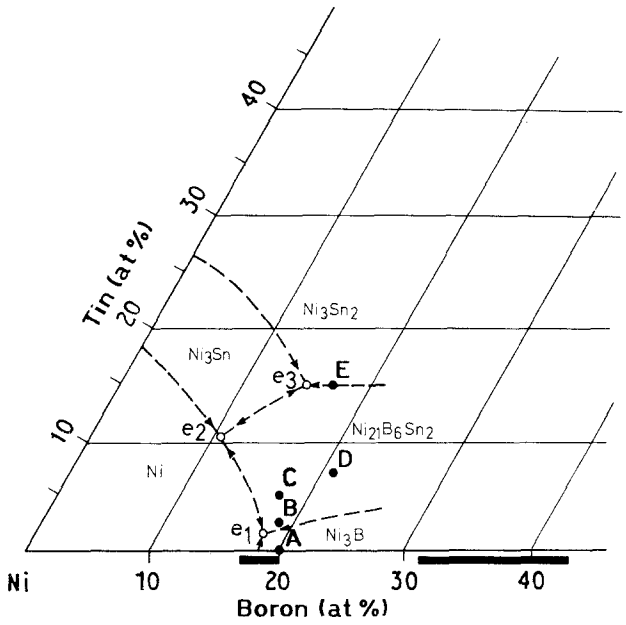

Figure 1 Projection of the liquidus surfaces in the nickel-rich corner of the Ni–B–Sn ternary system. e1, e2, e3, ternary eutectics; A, B, C, D, E, samples which were studied in the glass-forming composition range of the Ni–B system.

TABLE I Composition of the samples studied

Sample	Composition (at %)
A	$Ni_{80}B_{20}$
B	$Ni_{78.8}B_{18.8}Sn_{2.4}$
C	$Ni_{77.4}B_{17.4}Sn_{5.2}$
D	$Ni_{72.4}B_{20.7}Sn_{6.9}$
E	$Ni_{68}B_{17}Sn_{15}$

0022–2461/91 $03.00 + .12

3. Results and discussion

3.1. Optical microscopy, XRD and EPMA on the as-cast samples

Fig. 2 shows the results of optical microscopy and Table II shows the phases identified by XRD. These results are in accordance with the projection of the liquidus surface shown in Fig. 1. They confirm the presence of the equilibrium phase Ni_3B (Samples A and B).

Fig. 2a shows the presence of τ primary phase, Ni_3B–$Ni_{21}B_6Sn_2$ binary eutectic and Ni–$Ni_{21}B_6Sn_2$–Ni_3B ternary eutectic (point e1 in Fig. 1) in Sample B. The presence of the ternary compound $Ni_{21}B_6Sn_2$ as primary grains and as a white phase of the binary eutectic was checked by EPMA.

Fig. 2b shows the binary eutectic and the ternary eutectic in Sample B. The presence of nickel in the ternary eutectic was not detected by XRD. This may be explained by two facts: diffraction lines corresponding to nickel on the diffraction diagrams practically coincide with some of the XRD lines corresponding to τ phase, and the small quantity of nickel phase present compared to the τ phase is not enough to modify the intensity of the diffraction lines corresponding to the ternary compound.

TABLE II Phases identified on the XRD powder diagram in the as-cast material

Sample	Phases identified
A	Ni + Ni3B
B	Ni3B + Ni21B6Sn2
C	Ni + Ni21B6Sn2
D	Ni21B6Sn2
E	Ni3Sn2 + Ni21B6Sn2

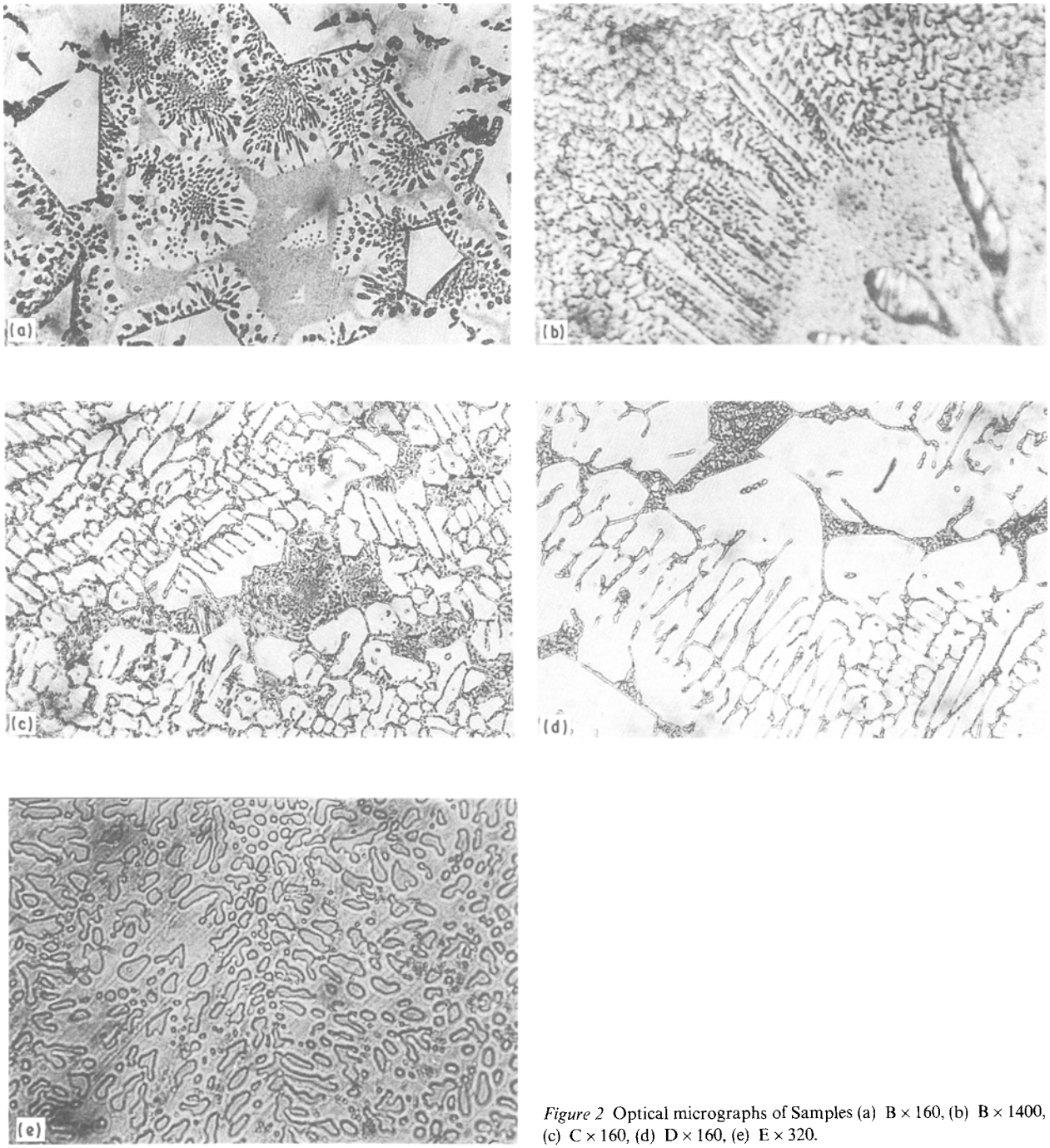

Figure 2 Optical micrographs of Samples (a) B × 160, (b) B × 1400, (c) C × 160, (d) D × 160, (e) E × 320.

Fig. 2c shows the presence of the $Ni_{21}B_6Sn_2$ primary grains and Ni–$Ni_{21}B_6Sn_2$ binary eutectic in Sample C. In this case nickel was detected by alteration of intensity of some of the XRD diffraction lines corresponding to $Ni_{21}B_6Sn_2$ compound.

Fig. 2d shows Sample D with the stoichiometric composition of the compound $Ni_{21}B_6Sn_2$. The presence of a second phase in small quantities (not identified by XRD) denotes small departures from the ideal stoichiometric compsition: 6.9 at % in tin [5]. The tin content in the primary grains of $Ni_{21}B_6Sn_2$ analysed by EPMA is approximately 6 at %.

Fig. 2e shows the presence of the binary eutectic formed by Ni_3Sn_2 and $Ni_{21}B_6Sn_2$ in Sample E.

3.2. XRD on as-quenched samples

Samples were prepared at two different quenching rates (ribbons of different average thickness) in order to compare their GFA. Table III shows the ribbon

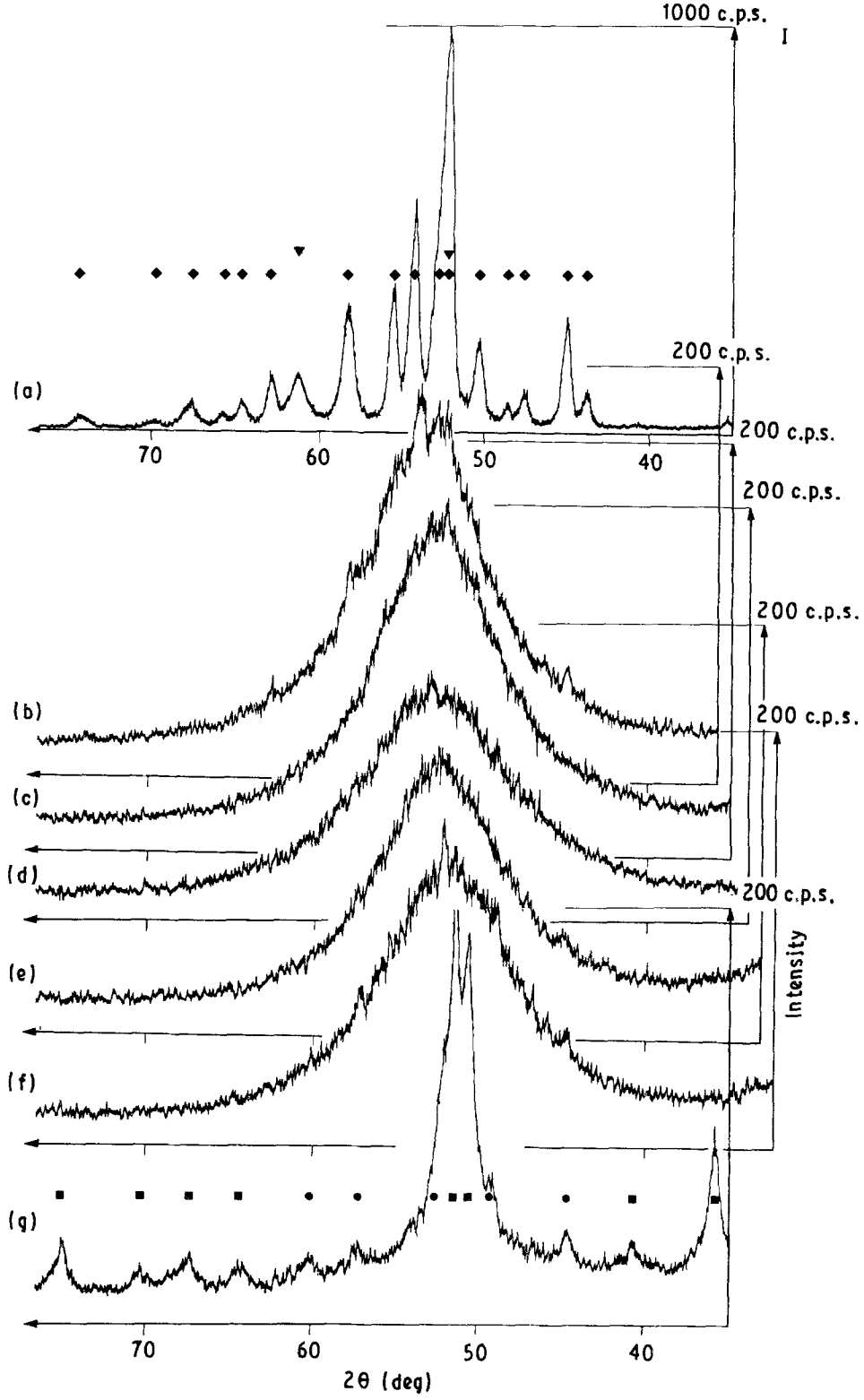

Figure 3 XRD patterns obtained with cobalt radiation in melt-spun samples. (a) 25 μm thick ribbon of Sample A, (b) 15 μm thick ribbon of Sample A, (c) 25 μm thick ribbon of Sample B, (d) 15 μm thick ribbon of Sample B, (e) 15 μm thick ribbon of Sample C, (f) 15 μm thick ribbon of Sample D, (g) 15 μm thick ribbon of Sample E. Identified phases: (◆) Ni_3B, (▼) Ni, (●) $Ni_{21}B_6Sn_2$, (■) Ni_3Sn_2.

TABLE III Thickness of the ribbons obtained by melt spinning and main features of the XRD pattern

Sample	Average thickness (μ)	X-ray features[a]
A	25	c
	15	a + t
B	25	a
	15	a
C	15	a
D	15	a + t
E	15	c

[a] a, amorphous structure; t, crystalline structure traces; c, crystalline structure.

average thickness and the main features of the XRD patterns obtained with the cobalt source. These patterns are shown in Fig 3.

The presence of a halo in the diffraction patterns obtained with the cobalt source was used to characterize the existence of amorphous structure (Fig. 3b–f). It can be said that crystalline structure traces are present when incipient diffraction lines corresponding to possible phases become observable superimposed on the halo pattern (Fig. 3b and f).

X-ray analysis performed on Sample A shows a crystalline structure on the 25 μm thick ribbon (Fig. 3a) and an amorphous structure with traces of crystalline phases on the 15 μm thick ribbon (Fig. 3b). In the 25 μm crystalline ribbon the equilibrium phases nickel and Ni_3B are present.

Similar studies on Sample B show amorphous structure on both ribbons (25 μm, Fig. 3c and 15 μm, Fig. 3d) characterized by a halo pattern centred in $2\theta = 52.8°$ (cobalt source). Comparing Fig. 3a and b with Fig. 3c and d, it can be concluded that the addition of tin increases the GFA of the system NiB.

Analysis of Samples C, D and E (15 μm thickness) suggests a glass-forming composition range. XRD patterns show that the melt-spun Samples C (Fig. 3e) and D (Fig. 3f) exhibit amorphous structures characterized by a halo pattern centred in $2\theta = 52.8°$ (Cobalt source) while the melt-spun Sample E (Fig. 3g) exhibits crystalline equilibrium phases Ni_3Sn_2 and $Ni_{21}B_6Sn_2$. Thus E represents an upper limit to the addition of tin in order to obtain amorphous phase.

The XRD pattern of melt-spun Sample E (Fig. 3g) shows weak lines corresponding to $Ni_{21}B_6Sn_2$ phase and strong lines corresponding to Ni_3Sn_2 phase, while the pattern of the as-cast Sample E shows intense lines for both Ni_3Sn_2 and $Ni_{21}B_6Sn_2$. This remarkable decrease of relative line intensity in the diffraction pattern of the melt-spun Sample E, together with the GFA of Sample D composed mainly of $Ni_{21}B_6Sn_2$, suggests that the nucleation and growth of $Ni_{21}B_6Sn_2$ crystal is not easily achieved. This fact may be related to the complex structure of the boride $Ni_{21}B_6Sn_2$ which needs the presence of tin atoms in very particular lattice positions as stabilizing elements [5]. Thus a glass-forming composition range can be thought of as extending through the $Ni_{21}B_6Sn_2$ primary phase field joining the two glass-forming composition ranges of the binary system. This idea is represented in Fig. 4.

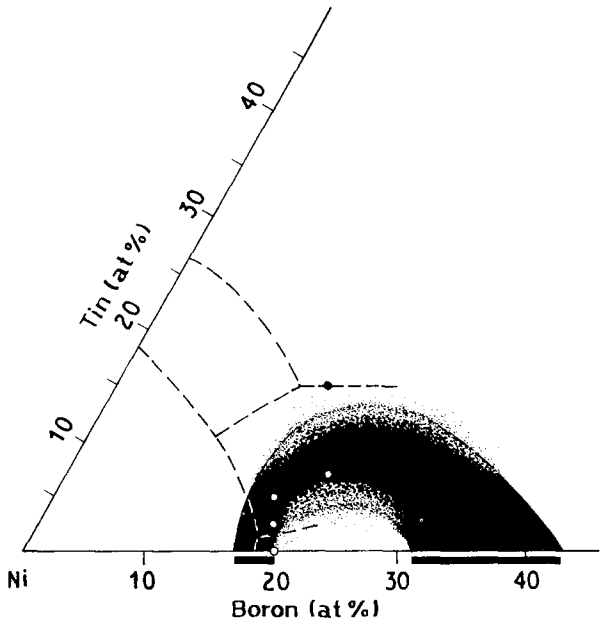

Figure 4 Presumed glass-forming composition range of the amorphous structure of the Ni–B–Sn system. (○) Amorphous samples, (●) crystalline sample.

TABLE IV Mössbauer parameters of Samples B and D

Sample	Isomer shift IS(± 0.02 mm s^{-1})	Quadrupole splitting Δ(± 0.02 mm s^{-1})
B melt-spun	1.54	0.62
B melt-spun, annealed at 200 °C for 8 h	1.54	0.61
B melt-spun, annealed at 300 °C for 6 h	1.53	0.63
B melt-spun, annealed at 400 °C for 4 h	1.51	0.63
B as-cast	1.48	—
D as-cast	1.48	—
D melt-spun	1.45	—
	1.56	0.67

This behaviour is observed in NiAlB [3] which also exhibits a τ phase $Ni_{21}B_6Al_2$.

3.3. Mössbauer spectroscopy

As-cast and as-quenched Samples B and D (15 μm average thickness ribbons) were analysed by Mössbauer spectroscopy. The crystallization behaviour of as-quenched Sample B (15 μm thick ribbons) was also studied by Mössbauer spectroscopy and XRD. The results are shown in Table IV, and Figs 5 and 6.

The environment of tin analysed by Mössbauer spectroscopy in as-cast Samples B and E results, in both cases, in an absorption spectrum characterized by a unique line with IS(B) = 1.48 ± 0.02 mm s^{-1} and IS(D) = 1.45 ± 0.02 mm s^{-1}, respectively (Figs 5e and 6a). These spectra are characteristic of the $Ni_{21}B_6Sn_2$ compound [6].

Both as-quenched Samples B and D exhibiting an amorphous structure have a tin environment characterized by an electric field gradient corresponding to a quadrupole splitting of 0.62 and 0.67 mm s^{-1}, respectively (Figs 5a and 6b). This local order is very stable as

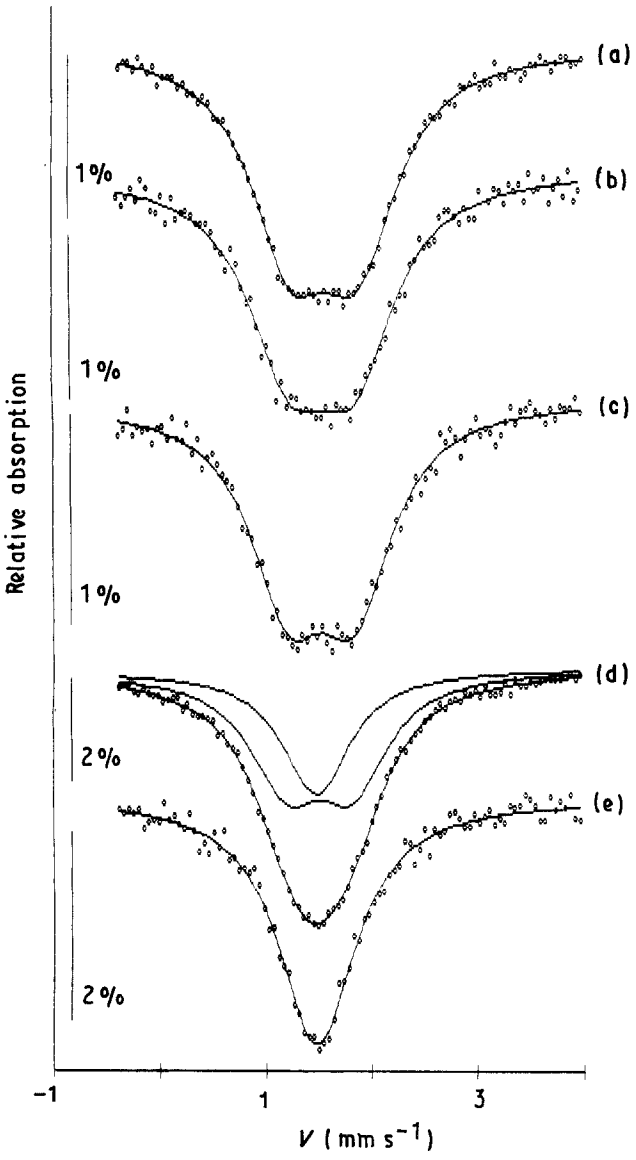

Figure 5 Mössbauer spectra in ribbons of Sample B. (a) Melt-spun; (b) melt-spun, annealed at 200 °C for 8 h; (c) melt-spun, annealed at 300 °C for 6 h; (d) melt-spun, annealed at 400 °C for 4 h; (e) as-cast.

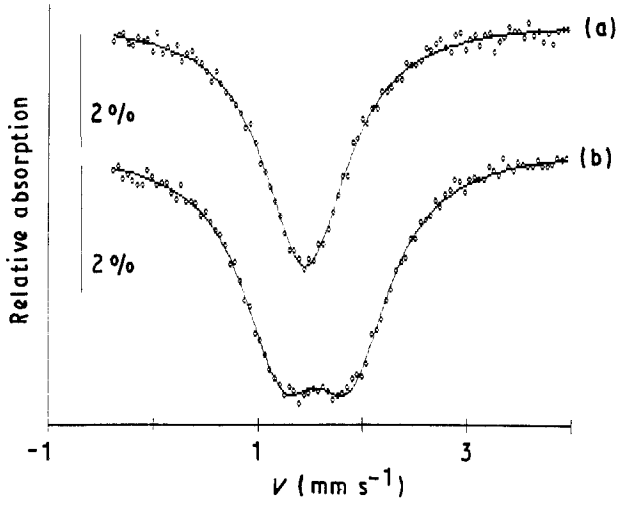

Figure 6 Mössbauer spectra in ribbons of Sample D. (a) As-cast, (b) melt-spun.

can be seen by the fact that it persists even after annealing for 6 h up to 300 °C (Fig. 5c). This temperature is higher than the crystallization temperature (220 °C) of ribbon samples of the NiB system with a composition around the eutectic at 18.4 at % in boron [7].

The spectrum obtained from Sample B annealed at 400 °C for 4 h is best fitted by a quadrupolar splitting similar to that present in the amorphous state, and a single line corresponding to the crystalline phase $Ni_{21}B_6Sn_2$ (Fig. 5d). This evidence of crystalline $Ni_{21}B_6Sn_2$ was verified by XRD; the diffraction pattern on the same sample shows intense lines attributable to Ni_3B (with distorted lattice) as the main phase and weak lines attributable to $Ni_{21}B_6Sn_2$. On the other hand, the as-cast diffraction pattern of Sample B shows intense lines corresponding to both Ni_3B and $Ni_{21}B_6Sn_2$. This remarkable decrease of the relative intensity of the τ phase in melt-spun samples relative to as-cast ones suggests that the nucleation and growth of $Ni_{21}B_6Sn_2$ crystal is not easily achieved (this suggestion has already been put forward in the previous section). A two-step crystallization process seems to take place during annealing, similar to that observed by Inoue *et al.* [3]

$$\text{amorphous} \rightarrow \text{amorphous} + Ni_3B$$
$$\rightarrow Ni_3B + Ni_{21}B_6Sn_2$$

4. Conclusions

The addition of small quantities of tin increases the GFA of the binary system. Glass formation is observed in the nickel-rich corner of the Ni–B–Sn ternary system for a tin content less than 15 at %. The glass-forming composition range seems to extend through the $Ni_{21}B_6Sn_2$ primary field joining the two formation ranges of amorphous phase of the Ni–B binary system. This fact may be related to the difficulty of formation of the ternary compound $Ni_{21}B_6Sn_2$ whose tin environment differs from that present in the amorphous state.

Acknowledgements

The authors thank Mr F. Audebert for the microscopic inspection and Lic. D. Hermida for obtaining the XRD patterns with the cobalt source.

References

1 H. SIRKIN, N. MINGOLO, E. NASSIF and B. ARCONDO, *J. Non-Cryst. Solids* **93** (1987) 323.
2. N. MINGOLO, E. NASSIF, B. ARCONDO and H. SIRKIN, *ibid.* **113** (1989) 161.
3 A. INOUE, A. KITAMURA and T. MASUMOTO, *J. Mater. Sci.* **16** (1981) 1895.
4. H. H. STADELMAIER and L. T. JORDAN, *Z. Metallkde* **53** (1962) 719.
5. H. H. STADELMAIER, in "Developments in the Structural Chemistry of Alloy Phases", edited by B. C. Giessen (Plenum Press, New York, 1969) p. 141.
6. H. Z. DOKUZOGUZ, H. H. STADELMAIER and L. H. BOWEN, *J. Less-Common Metals* **23** (1971) 245.
7. M. TAKAHASHI, Y. TATENO and M. KOSHIMURA, *Jpn J. Appl. Phys.* **19** (1980) 2335.

Received 4 October 1990
and accepted 20 March 1991